Desalination and Water Treatment
www.deswater.com
doi: 10.5004/dwt.2023.29306

285 (2023) 129–145
February

Studies on the adsorptive removal of cesium ions using *Nigella sativa* as an adsorbent and optimization with response surface modeling

Edward Kavitha*, R.B. Balayogesh, Abraham Roshan, A.S. Adwaid, Satapathy Mrityunjay

Department of Chemical Engineering, College of Engineering and Technology, SRM Institute of Science and Technology, Potheri, Kattankulathur 603203, Chengalpattu District, Tamil Nadu, India, Tel.: +91-9445609098; email: kavi0910@gmail.com (E. Kavitha), Tel.: +91-9207589702; email: balayogesh998@gmail.com (R.B. Balayogesh), Tel.: +91-9819791248; email: rosabraham8@gmail.com (A. Roshan), Tel.: +91-7025665433; email: adwaid169@gmail.com (A.S. Adwaid), Tel.: +91-8280476982; email: mrityunjay.satapathy97@gmail.com (S. Mrityunjay)

Received 22 October 2022; Accepted 18 January 2023

ABSTRACT

The wastewater contaminated with radioactive wastes is more hazardous and has an adverse impact on ecosystems. One of the harmful species present in radioactive wastes is cesium. We are in need of adequate process for the removal of cesium to protect the environment. In recent years, the adsorption process has been adopted for the removal of contaminants from the waste stream. In this study, a new low-cost adsorbent synthesized from *Nigella sativa* (black cumin seed) has been employed for the removal of Cs(I) from the simulated wastewater. The adsorbent was characterized by scanning electron microscopy, energy-dispersive X-ray, X-ray diffraction, and Fourier-transform infrared spectroscopy analysis. The simulated wastewater sample containing cesium ions was prepared and the adsorption studies were carried out. The process parameters such as initial solution pH, contact time, the dosage of adsorbent, and concentration of Cs(I) were examined and the percentage separation of Cs(I) and adsorption capacity of activated black cumin seed (BCS) were evaluated. The kinetic studies and adsorption isotherm studies were performed to analyze the experimental findings. The optimized parameters were evaluated using the Response surface methodology to analyze the maximum percentage removal of Cs(I) and adsorption capacity of activated BCS. The optimized values were compared with the experimental findings.

Keywords: Adsorption; *Nigella sativa*; Cesium; Radioactive wastes; Low-cost adsorbent

1. Introduction

The ecological and environmental impact of radioactive wastes in the aqueous stream has attracted attention worldwide towards the safe treatment and disposal of radioactive wastes. Nuclear power has been employed in nuclear power generation, mining, research and medical applications, etc. The byproducts of the nuclear fuel cell, and also the radioactive materials utilized in other fields such as research, and medicine are considered to be radioactive wastes [1]. Due to the rapid development of nuclear power applications, the disposal of various levels of radioactive waste has become a great concern for the environment and public health. Based on the activity and the concentration, the radioactive wastes are grouped as low, intermediate, and high-level wastes. The half-life of most of the radionuclides is more and it takes a long period for degradation. The safe handling, treatment, and disposal of the contaminants is the crucial part concerning radionuclides.

Among the radioactive wastes, cesium is one of the harmful species. It is one of the chief components of fission products, and it has become the prime nuclide to be

* Corresponding author.

Presented at the 1st International Virtual Conference on Sustainable Water 2022 (ICSW 2022), 22–23 March 2022, organized by KPRIET, Coimbatore, India

1944-3994/1944-3986

removed from the effluent [2]. There are various stable forms of cesium and the most common radionuclide of cesium is Cs^{137}. It is commonly found as the by-product of nuclear fission processes and it is also highly soluble in water [3]. The half-life period of Cs^{137} is 30 y and which is quite a long period. It indulges in serious environmental impacts due to the emission of high energy gamma radiation [3,4]. The long term exposure to this radionuclide can lead to the risk of cancer. When the cesium ions enter the human body, it creates harmful effects. So, it is an environmental need to develop a suitable technology for the treatment of cesium ions in the liquid effluent. However, cesium finds wide applications in the medical field, atomic clock, solar devices, electronic items, etc. [5,6].

There are various conventional treatment methods such as chemical precipitation [7], adsorption [8,9], ion exchange process [7,10], liquid–liquid extraction [11,12], electrochemical process [13], membrane separation process [14] for the treatment of radioactive wastes. The ion exchange process is the widely employed separation methodology for the removal of cesium radionuclides. However, this process lacks due to the competitive impact of other ions of sodium and potassium present in the wastewater which impedes the ionic interaction of cesium with ion exchange resins [3]. So, it requires the synthesis of a suitable resin for getting the selective separation of cesium. Electrochemical treatment is an emerging trend that could effectively separate cesium ions without the generation of secondary pollutants. However, this process lacks its wider applications due to the difficulty in electrode fabrication [15]. Membrane separation processes are well known for their selective separation of ions. However, there is a problem of membrane fouling and exploitation of membrane due to radiation [15]. The photocatalytic processes have also been attempted by many researchers in recent years, owing to their ease of operation, and efficiency [16]. Amid of all these processes, ease of operation and efficiency make the adsorption process more advantageous. Recently, the application of functionalized nanomaterials in the adsorption process has becoming the emerging technology for the separation of heavy metal ions [17,18].

In the past few decades, there has been increasing attention towards the adsorptive removal of radioactive wastes as a better alternative to other conventional treatment methods. Several synthetic adsorbents and biosorbents were investigated for the adsorptive separation of cesium ions contaminated liquid effluent. For the removal of Cs(I) from the aqueous stream the following adsorbents were reported in the literature: Prussian blue analogues [19], titanate-based adsorbents [20], molybdophosphate [21], tungstophosphate [22], PAN-based adsorbers [23], AMP – calcium alginate composite [24], functionalized montmorillonite clay [25], dual functional micro adsorbents [26], magnetic chitosan [27].

In the past few decades, there were a lot of research on the development of low-cost, eco-friendly adsorbents for the treatment of toxic heavy metals from wastewater. Globally, a lot of work was carried out using biomaterials as an adsorbent for the separation of toxic pollutants from waste streams [28]. The adsorbents synthesized from biomaterials such as de-oiled soya [29], bagasse fly ash [30], bamboo [31], rice husk [32], rice straw [33], coconut shell [34], palm kernel shell [35], chitosan based nano adsorbents [36], etc have been reported in the literature. We are in need of an adequate technology for the treatment of toxic and hazardous metal ions, which could overcome the drawbacks of the conventional processes such as selective separation, cost of synthesis of resins and adsorbents, recovery and reuse of the resins and adsorbents, fabrication of suitable electrodes, generation of secondary pollutants, membrane fouling, etc [37,38]. This present study is aimed to cover these gaps by adopting adsorptive removal of cesium ions using the adsorbent *Nigella sativa* (black cumin seed).

The black cumin seed (BCS) is a well-known home medicine, which has a bitter taste and pungent flavour. It is widely used for medicinal purposes in India, Arab, and Africa. It has been used as an analgesic, anti-inflammatory, and anti-oxidant medicine. It has been chosen as an adsorbent owing to its abundance and cost, eco-friendliness, reusability, hydroxyl, carboxyl, and amide groups in it. All these characteristics exhibit it as a potential adsorbent for the removal of Cs(I) from the liquid waste. The novelty of this study involves the application of activated black cumin seeds as an adsorbent to remove Cs(I). Many of the works reported earlier focused only on the separation of heavy metal ions using activated BCS. This paper deals with the separation of Cs(I) and also the experimental findings were analyzed with the kinetic and isotherm studies. The characterization of the activated BCS was also carried out by scanning electron microscopy analysis (SEM), energy-dispersive X-ray analysis (EDX), Fourier-transform infrared spectroscopy analysis (FTIR), and X-ray diffraction analysis (XRD).

The batch experiments were executed by varying the parameters initial pH, time of adsorption, the dosage of activated BCS, initial concentration of Cs(I), and temperature. The characterization of activated BCS before and after adsorption studies was performed. The kinetic and adsorption isotherm studies were performed. Based on the preliminary batch experimental results, the design of experiments was accomplished by response surface methodology (RSM) (Design-Expert 10.0.0). RSM is a well-known mathematical, and statistical tool, for process modeling and optimization. By appropriate experimental design, RSM generates the relation of response to the various levels of input parameters. This involves screening of variables, fixing the lower and upper levels of process variables, design of experiments, analysis of variables, and optimization of process variables. The various levels of process parameters are grouped to fit the second-order polynomials to the measured outcome. In this work, the experiments were executed by the central composite design tool, and the process responses percentage removal of Cs(I) and adsorption capacity of activated BCS were evaluated. The process modeling and optimization of process parameters were performed.

2. Materials and methods

2.1. Chemicals

$CsNO_3$ was used to prepare the stock solution of 100 ppm concentration. Black cumin seeds were used as the base material for the preparation of adsorbent. The reagents H_2SO_4, NaOH, and HCl were used in the adsorbent preparation and also in the adsorption studies. The analytical

grade reagents and distilled water were utilized for the experimental studies.

2.2. Adsorbent preparation [28,39]

100 g of BCS was taken and cleaned with water. BCS was dried and ground into a fine powder. Then the chemical activation of the adsorbent was performed. The concentrated solution of H_2SO_4 (100 mL) was added in the range of 1:1 (w/w) drop by drop to the fine powder of BCS. It was stirred well and kept in an oven at 150°C for about 18 h for drying. After complete drying, it was crushed and then the pH was brought to a neutral level by washing with water. Again, it was dried, weighed and stored in a container. The yield was found to be 75%. Fig. 1 shows the black cumin seed and activated BCS samples.

2.3. Activated BCS characterization studies

After adsorbent preparation, the sample of activated BCS was taken for characterization studies. Another sample of activated BCS was taken after performing the adsorption studies for the characteristics analysis. The surface morphology of the activated BCS before and after adsorption studies were analyzed by scanning electron microscopy (SEM, Thermo Fisher Scientific, Apreo 8). The elemental composition before and after adsorption studies was analyzed to ensure the removal of Cs(I) on the surface of activated BCS, by EDX. The crystalline nature of the activated BCS was analyzed by XRD (Bruker USA D8 Advance, Davinci). FTIR (Shimadzu, IRTracer – 100) analysis was done to analyze the functional groups in activated BCS. The pore radius, volume, and average surface area were determined by Brunauer–Emmett–Teller (BET) analysis (Quantachrome Instruments, Autosorb IQ series).

2.4. Adsorption studies

The feed solution of various concentrations of cesium in the range of 2–10 mg/L of 50 mL volume was taken in a glass beaker. Then the adsorbent was added in the range of 0.25–2 g, and the initial solution pH was maintained between 2 and 12 by adding buffer solution. The beaker was sealed and kept in an orbital shaker. The solution was shaken in the orbital shaker at a speed of 140 rpm. The time of shaking was maintained between 4–120 min. After the shaking process, it was vacuum filtered and the sample of the filtrate was taken for analysis by ICP-MS to evaluate the concentration of cesium in it. The schematic representation of the process is shown in Fig. 2.

2.5. Kinetic studies

The experiments were performed to analyze the influence of contact time, initial pH, the dosage of activated BCS, and the concentration of Cs(I). The experimental data were validated by kinetic and isothermal studies. The percentage removal of Cs(I) and adsorption capacity of activated BCS were evaluated by the following equations:

The percentage removal of Cs(I) was calculated using Eq. (1).

$$\text{The percentage removal of } \mathrm{Cs(I)} = \frac{\left(C_0 - C_e\right)}{C_0} \times 100 \tag{1}$$

The adsorption capacity of activated BCS was determined using Eq. (2).

$$\text{The adsorption capacity of BCS, } Q_e = \frac{\left(C_0 - C_e\right)V}{w} \tag{2}$$

where C_0 = initial concentration of cesium, mg/L; C_e = final concentration of cesium, mg/L; Q_e = adsorption capacity of activated BCS, mg/g; V = volume of feed solution, L; W = mass of activated BCS, g

2.6. Kinetic modeling and adsorption isotherm studies

The experiments were performed at the various initial concentration of Cs(I), initial pH, contact time, the dosage of activated BCS, and temperature. The pseudo-first-order and pseudo-second-order modeling equations were analyzed with the experimental findings and the proper fit was evaluated. The fitness of the experimental data with the following adsorption isotherm was evaluated: Langmuir, Freundlich, and Dubinin–Radushkevich under specified operating conditions.

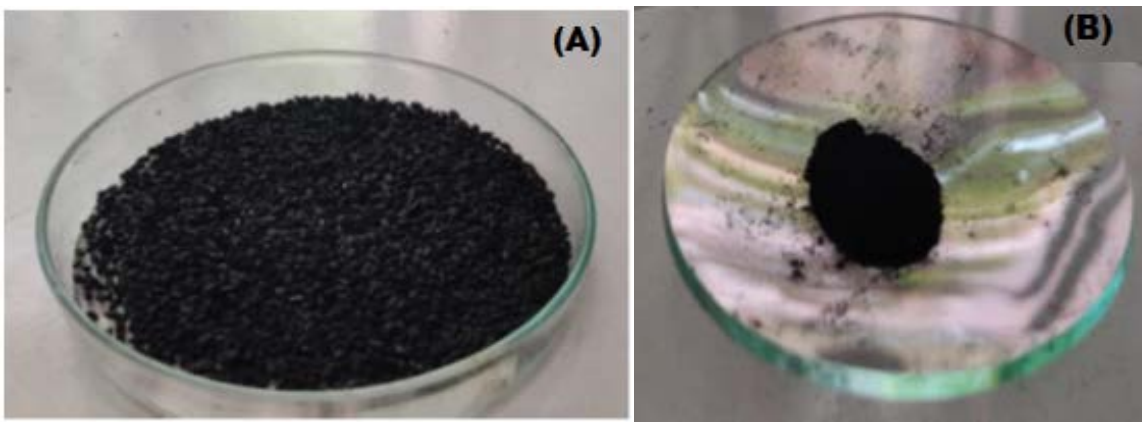

Fig. 1. (A) Black cumin seed and (B) activated black cumin seed sample.

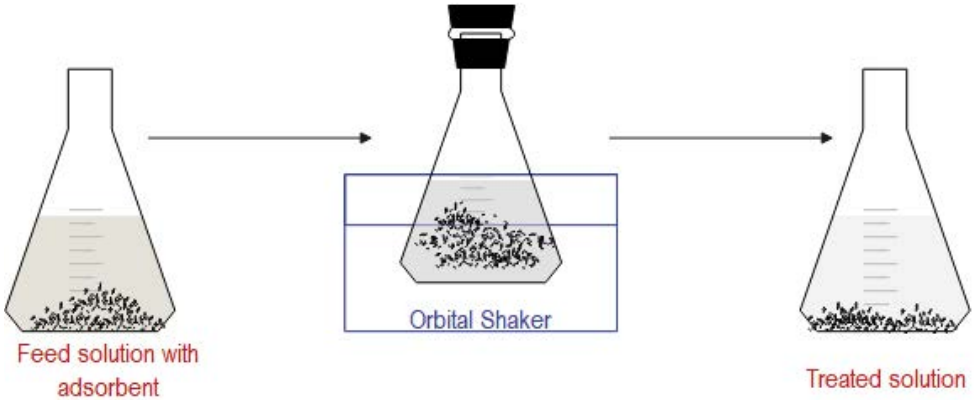

Fig. 2. Schematic representation of batch adsorption study.

2.7. Design of experiments

The process modeling and optimization were performed by RSM. It involves the mathematical approach to obtain the empirical relation between the process variables and responses [40]. The following steps are adopted in this approach: screening of variables, design of experiments, analysis of variance (ANOVA), and process optimization. This methodology minimizes the number of experimental runs to be performed and also evaluates the interactive effect of process variables on the responses [41]. The central composite design (CCD) tool of RSM was adopted for the design of experiments. The screening of variables was done based on the literature and parameters initial pH, the dosage of activated BCS, the concentration of Cs(I), and contact time [42,43] were chosen. The experiments were performed and the process responses such as percentage adsorption of Cs(I) and adsorption capacity of activated BCS were calculated.

To fit the experimental data, a second-order polynomial model equation was generated and was represented by Eq. (3) [44,45].

$$\hat{Y} = b_0 + \sum_{i=1}^{k} b_i x_i + \sum_{i=1}^{k} b_{ij} x_i^2 + \sum_{i=1}^{k} \sum_{j=1}^{j \le i} b_{ij} x_i x_j \quad (3)$$

where $\hat{Y}$ denotes the predicted process responses percentage adsorption of Cs(I), and adsorption capacity of activated BCS. x_i denotes the coded levels of the process variables. b_0, b_i, b_{ii}, b_{ij} are the regression coefficients evaluated by least square regression (offset term, main, quadratic, and interaction effects).

3. Results and discussion

3.1. Physical characterization of activated BCS by SEM, EDX, FTIR, and XRD analysis

The surface features and elemental composition of the activated BCS were analyzed through SEM and EDX. The activated adsorbent sample before and after adsorption studies was taken and dried at room temperature. Fig. 3a and b exhibit the SEM images of the activated BCS. It clearly shows the pores created on the surface of the activated BCS. Fig. 3c and d show the images of the activated BCS surface after performing adsorption studies. It is observed from the images Fig. 3a–d that there is a changeover in the surface morphology of the activated BCS after performing adsorption. The composition of elements in activated BCS respective to pre-adsorption and post-adsorption studies is shown in Fig. 4a and b. The peak corresponding to Cs in Fig. 4b confirms the adsorption of Cs(I) over the active sites of the activated BCS.

Fourier transform infrared is a widely applied technique to analyse chemical compounds and their structure. The FTIR spectrum for the activated BCS before and after adsorption studies has been illustrated in Fig. 5. The peak corresponds to the 1,150 mm^{-1} refers to the C–OH stretch. The wavelength 2,923 and 2,853 mm^{-1} corresponds to –CH stretch of $–CH_3$ and $–CH_2$, respectively [28]. The presence of amide group consisting of –C=O and $–NH_2$ is represented by the bands at 1,702 and 1,457 mm^{-1}, respectively [28]. The functional groups in activated BCS remain unaltered before and after adsorption studies. The interaction between the adsorbent surface and Cs(I) was by electrostatic attraction.

XRD analysis is carried out to determine the crystalline structure of the adsorbent and it is a non-destructive technique. The activated BCS was analyzed by XRD to evaluate its crystalline nature. The sample of activated BCS after undergoing adsorption studies was also examined. From the analysis results, as shown in Fig. 6a and b, it is revealed that there is no change in of crystalline nature of the activated BCS.

3.2. Zero-point charge (pHzpc)

Zero-point charge refers to the pH at which the adsorbent's net surface charge becomes null. It is an important characterization of the adsorbent for finding its efficiency to adsorb cations and anions. At acidic pH, the H^+ will be adsorbed more compared to the cationic adsorbate. So, the adsorption capacity will be less when the surface is negatively charged. At higher pH, when the surface of the adsorbent is positively charged, OH^- will be adsorbed more and the anionic adsorbate will be less adsorbed. The ZPC of the activated BCS was found to be 2.5. Hence, the adsorbent surface is negatively charged if the pH is above this

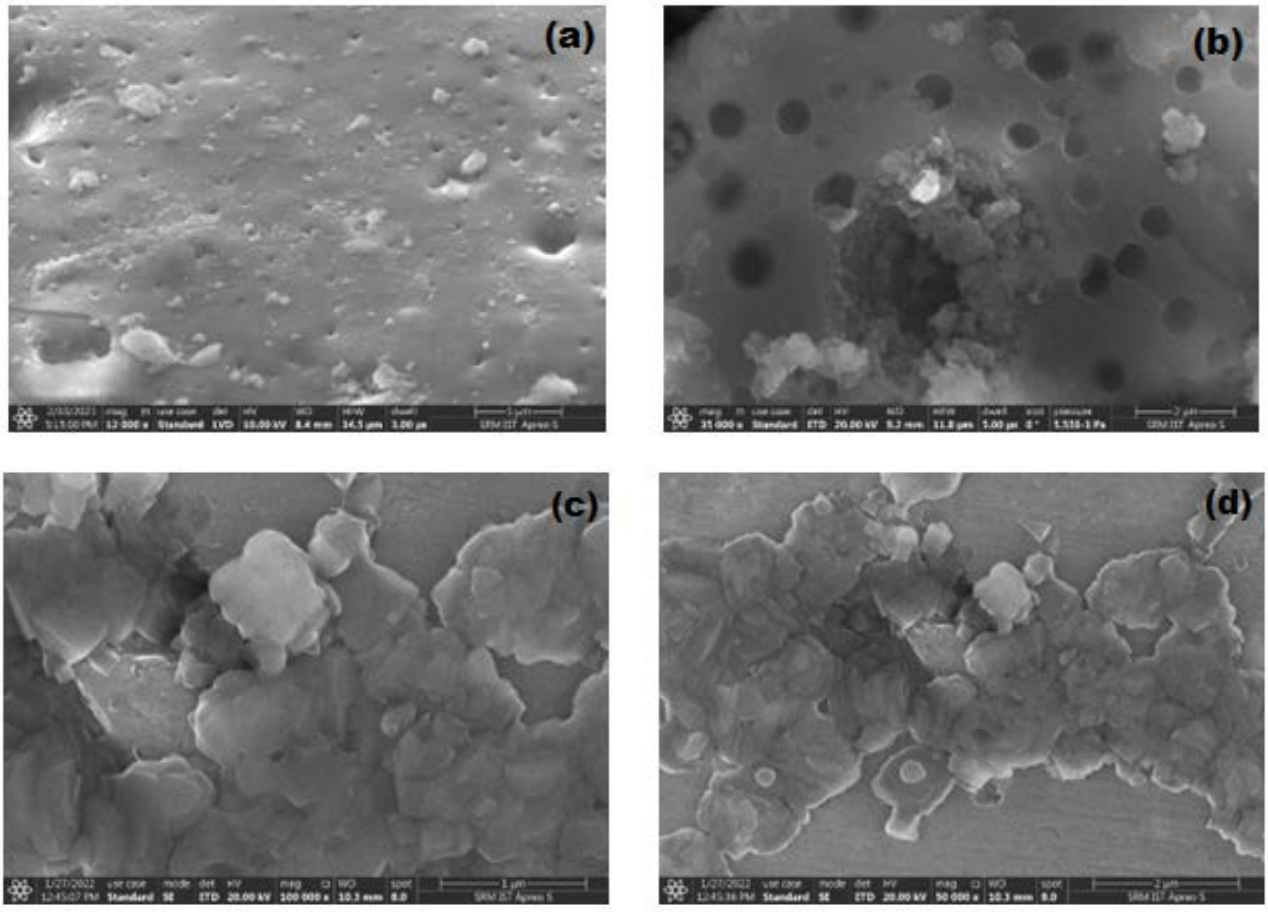

Fig. 3. (a, b) SEM image of activated BCS and (c, d) SEM image of activated BCS after performing adsorption studies.

value and more cations could be adsorbed on its surface. The surface is positively charged with lower pH and more anions could be attracted to the surface of the adsorbent.

3.3. Brunauer–Emmett–Teller (BET) analysis

The sample of activated BCS was analyzed to evaluate the pore size, volume, and surface area. The following data were obtained from the analysis: Average surface area of the adsorbent – 38.97 m^2/g, pore volume – 0.079 cm^3/g, and the average pore radius – 15.269 Å. The analysis report exhibits that the adsorbent has a significant pore volume and also the surface area to trap the cesium ions.

3.4. Effect of time on adsorption

A set of experiments was performed to investigate the influence of time on adsorption. The percentage removal of Cs(I) and adsorption capacity of activated BCS were evaluated at the contact time in the range of 4–120 min. The influence of contact time on the percentage removal of Cs(I) is shown in Fig. 7. It is observed from Fig. 7 that up to 16 min the percentage removal increases gradually. Then there is a steep increase in the percentage removal followed by a stable removal of Cs(I).

3.5. Effect of initial solution pH

The effect of the solution pH on the percentage removal of Cs(I) and adsorption capacity of activated BCS was investigated at various initial pH in the range of 2–12 at equilibrium contact time. It is exhibited from Fig. 8 that the percentage removal of Cs(I) increases with pH and beyond pH 10 there is no substantial increase. As the solution pH increases the active sites on the activated BCS surface acquire a negative charge and the electrostatic attraction between the adsorbent surface and the adsorbate increases. The –COOH, –OH and $–NH_2$ groups present in the adsorbent surface facilitates the electrostatic attraction between the adsorbent and Cs(I). It is also observed from the zero-point charge, that the intake of the cesium ions is more pronounced at higher pH.

3.6. Effect of dosage of activated BCS

The influence of dosage of activated BCS on the removal of Cs(I) and adsorption capacity of activated BCS was studied in the range of 0.25–2 g at optimum pH 10. Fig. 9 exhibits the increasing trend of percentage removal of Cs(I) with increasing adsorbent dosage. Since more active pores are available, the percentage removal of Cs(I) increases. However, beyond 1.5 g of adsorbent dosage, the increase

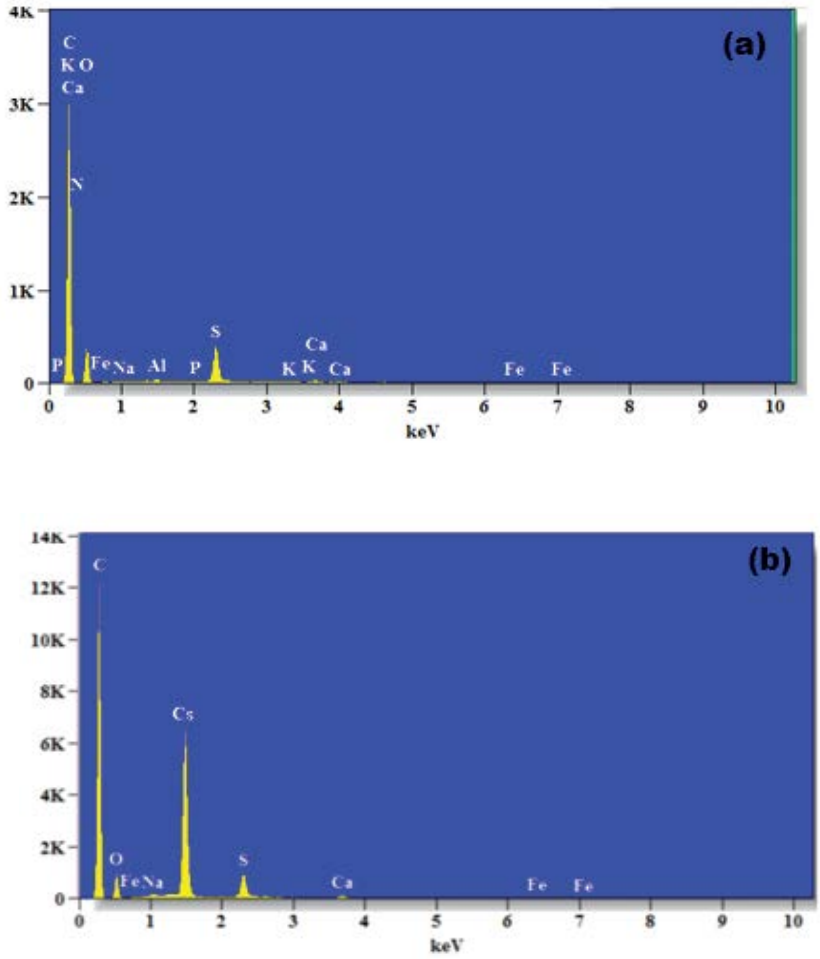

Fig. 4. EDX spectra of (a) activated BCS and (b) activated BCS after performing adsorption studies.

in the percentage removal is not substantial, due to the inadequate availability of Cs(I).

3.7. Effect of concentration of Cs(I)

The influence of cesium concentration on the percentage removal and the adsorption capacity of BCS was studied and Fig. 10 shows the observations on the influence of the cesium concentration on the percentage removal. The concentration of Cs(I) has a significant influence on the removal of Cs(I) as represented in Fig. 10. The percentage of removal increases from 25%–47%, with the increase in concentration from 2–8 mg/L. However, there is a steep increase in the removal of Cs(I) with a further increase in the initial concentration, due to the availability of cesium ions to get trapped by the activated BCS.

3.8. Kinetic modeling of experimental data

3.8.1. Pseudo-first-order reaction model

The experimental data were analyzed to evaluate the reaction model. The rate constant for the adsorption process was evaluated through the pseudo-first-order equation. Generally, Lagergren pseudo-second-order equation was employed to evaluate the adsorption of a liquid–solid system [46,47]. The linear form of the equation is represented using Eq. (4).

$$\ln\left(Q_e - Q_t\right) = \ln Q_e - k_1 t \tag{4}$$

where Q_e is the adsorption capacity at equilibrium condition, Q_t is the adsorption capacity at time t and k_1 is the first-order rate constant. The plot of $\ln(Q_e - Q_t)$ vs. contact time was plotted as shown in Fig. 11 to evaluate the rate constant k_1 and also theoretically Q_e. The values of k_1 and Q_e were evaluated from the slope and intercept, respectively. The regression coefficient was observed to be very less for the pseudo-first-order kinetic model and also a difference was observed between the theoretical and experimentally found values of Q_e. From these observations, it was found that the fit of experimental data with the pseudo-first-order kinetic model is poor.

3.8.2. Pseudo-second-order reaction model

The linear form of pseudo-second-order model equation is represented using Eq. (5).

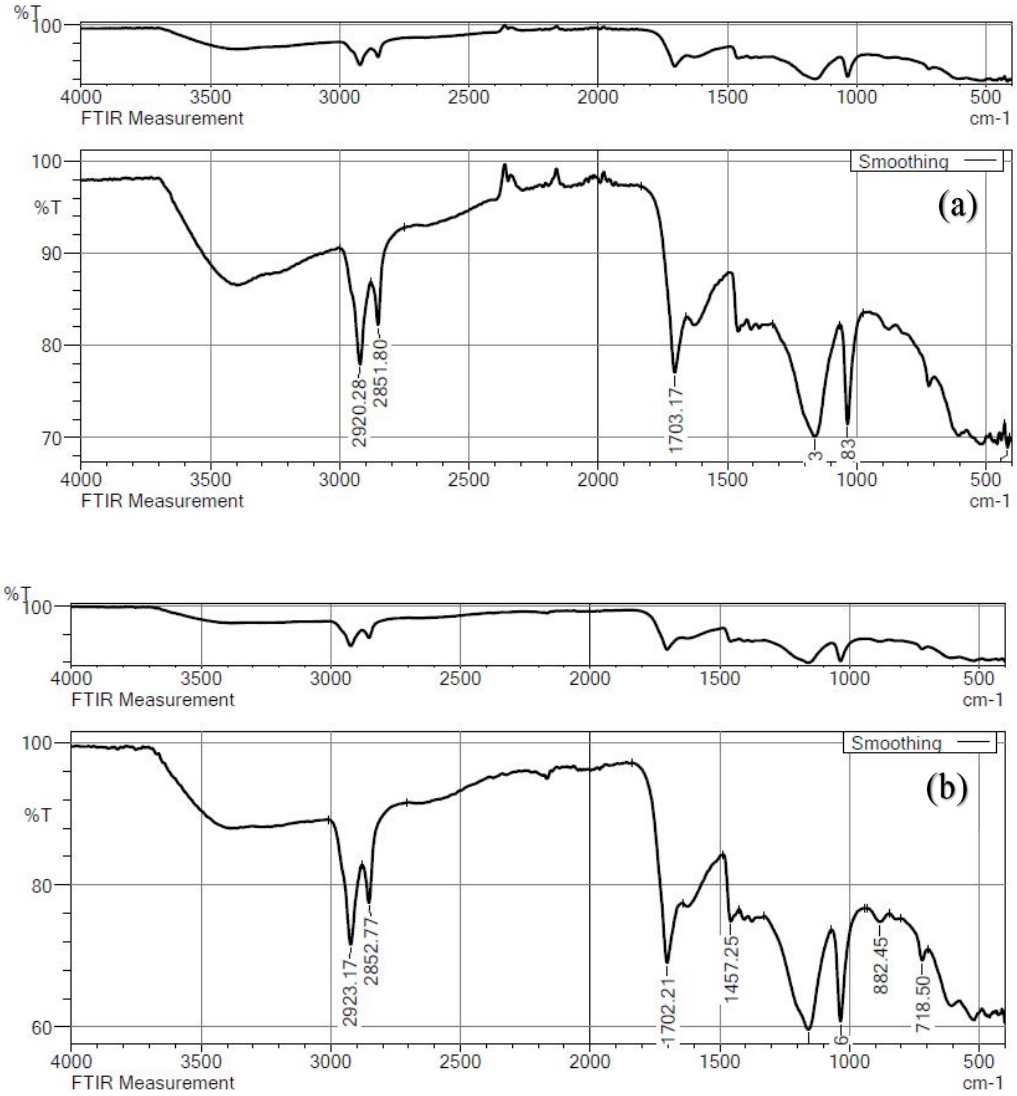

Fig. 5. FTIR spectra of (a) activated BCS and (b) activated BCS after performing adsorption studies.

$$\frac{T}{Q_t} = \frac{1}{k_2 Q_e^2} - \frac{1}{Q_e} t \tag{5}$$

where k_2 is the pseudo-second-order rate constant. The plot has been made between t/Q_t and time t as shown in Fig. 12. The values of k_2 and Q_e values were found from the slope and intercept of the graph [48]. The regression coefficient value is significant which indicates the fit of experimental results with the pseudo-second-order kinetics. The adsorption kinetics follows pseudo-second-order and the rate controlling step involved in this adsorption process is the chemical mechanism.

3.9. Adsorption isotherm studies

3.9.1. Langmuir adsorption isotherm

Adsorption isotherm studies are used to analyze the relation between the amount of adsorbent and the adsorbate concentration in the solution at equilibrium conditions and constant temperature. The mechanism of adsorption, adsorbent surface properties, and the interaction between the adsorbent and adsorbate are studied through an adsorption isotherm. The Langmuir adsorption isotherm relates to the equilibrium concentration of adsorbate when the adsorption is limited to mono-layer surface coverage [49,50]. The Langmuir adsorption isotherm in linear form is given by Eq. (6).

$$\frac{C_e}{Q_e} = \frac{1}{K_L Q_{\max}} + \frac{C_e}{Q_{\max}} \tag{6}$$

where C_e is the equilibrium concentration of Cs(I), Q_e is the equilibrium concentration of Cs(I) in the adsorbent, $Q_{\max}$ is the maximum adsorption capacity and K_L is the law constant [47].

The isotherm studies were performed at various temperatures between 30°C and 50°C. The graph between C_e/Q_e

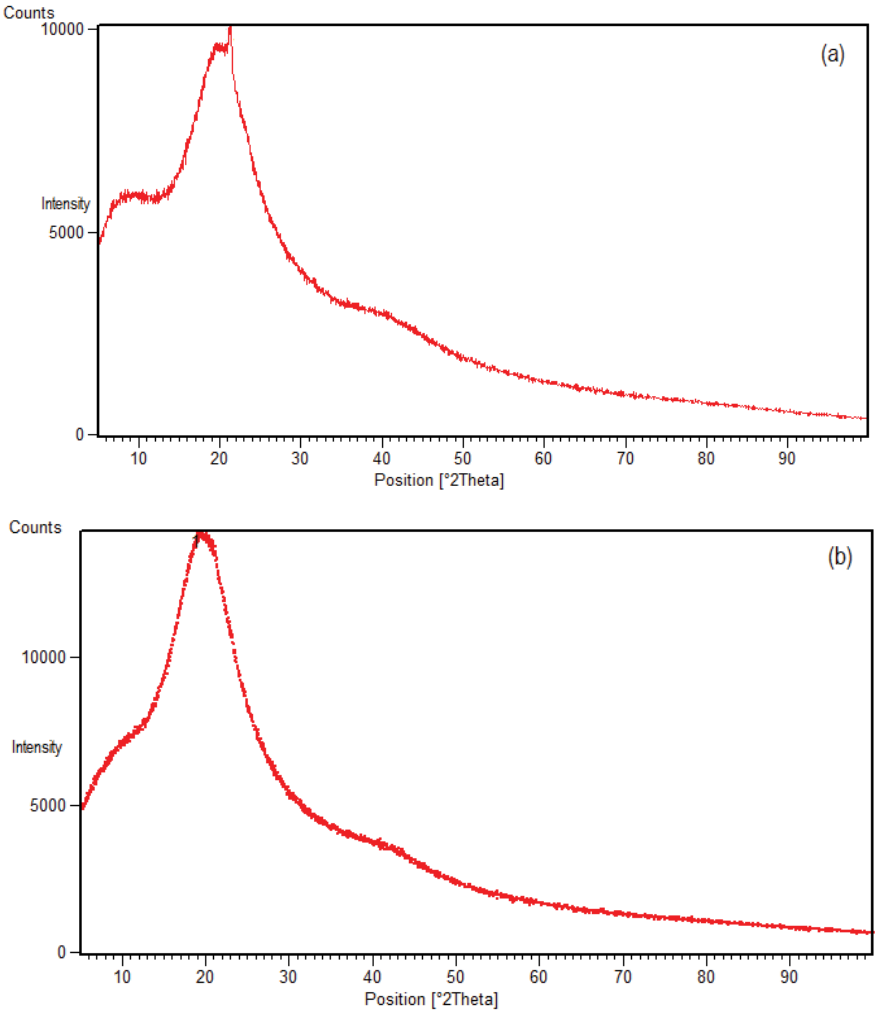

Fig. 6. XRD analysis of (a) activated BCS and (b) activated BCS after performing adsorption studies.

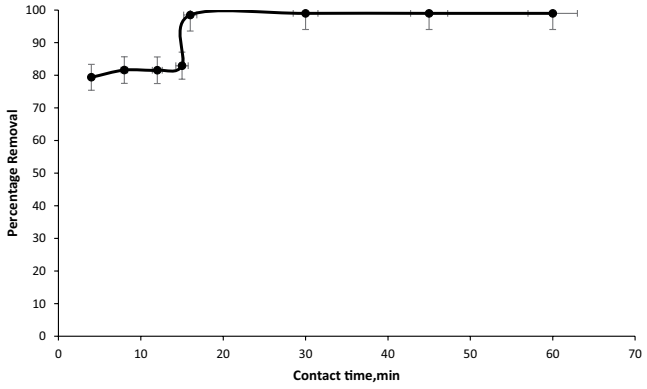

Fig. 7. Effect of contact time on the percentage removal of Cs(I). 50 mL of feed solution at ambient temperature.

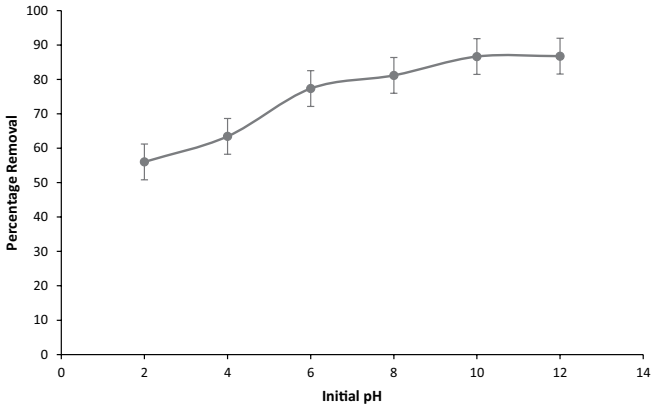

Fig. 8. Effect of initial pH on the percentage removal of Cs(I). 50 mL feed solution at equilibrium time.

vs. C_e as shown in Fig. 13 is plotted to analyze the Langmuir isotherm and from the graph, it is observed that there is a linear relation between C_e/Q_e and C_e for the experimental findings. This confirms the proper fit of the data and the values of Q_{max} and K_L from the chart are shown in Table 1.

The constant K_L is used to calculate the dimensionless separation factor which allows checking the feasibility of the process. The process is feasible when the value of R_L is between 0 and 1.

The dimensionless factor R_L is given by Eq. (7) [50].

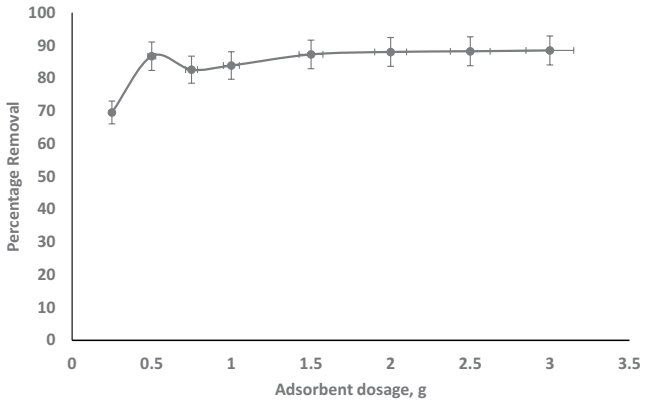

Fig. 9. Effect of adsorbent dosage on the percentage removal of Cs(I). 50 mL of feed solution at equilibrium time and optimum pH.

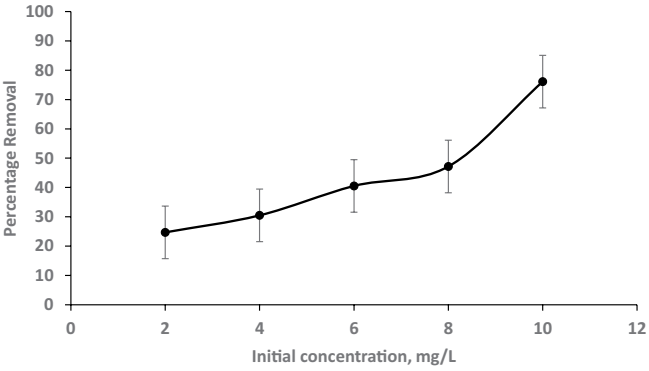

Fig. 10. Effect of initial concentration of Cs(I) on the percentage removal of Cs(I). 50 mL of feed solution at equilibrium time, optimum pH and adsorbent dosage.

$$R_L = \frac{1}{1 + K_L C_e} \tag{7}$$

The calculated values were between 0 and 1 representing the fitness of the experimental results with the Langmuir isotherm.

3.9.2. Freundlich adsorption isotherm

The Freundlich adsorption isotherm is an empirical model representing the relation between the adsorption capacity and pressure at a constant temperature. For the non-ideal adsorption processes taking place on nonuniform surfaces, the Freundlich adsorption isotherm could be applied. The Freundlich adsorption isotherm is given by Eq. (8).

$$\ln Q_e = \ln K_F + \frac{1}{n} \ln C_e \tag{8}$$

where K_F is the coefficient of Freundlich isotherm and n is the adsorption constant.

The plot of $\ln Q_e$ vs. $\ln C_e$ was made as shown in Fig. 14 to analyze the fitness of the experimental results with the

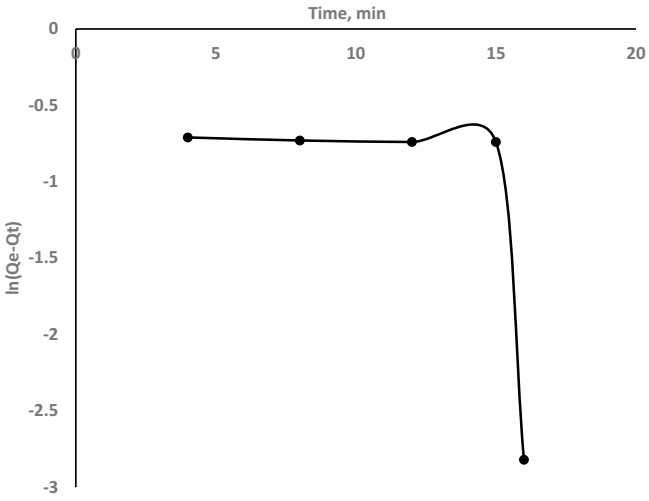

Fig. 11. Pseudo-first-order reaction kinetics: plot of $\ln(Q_e - Q_t)$ vs. contact time.

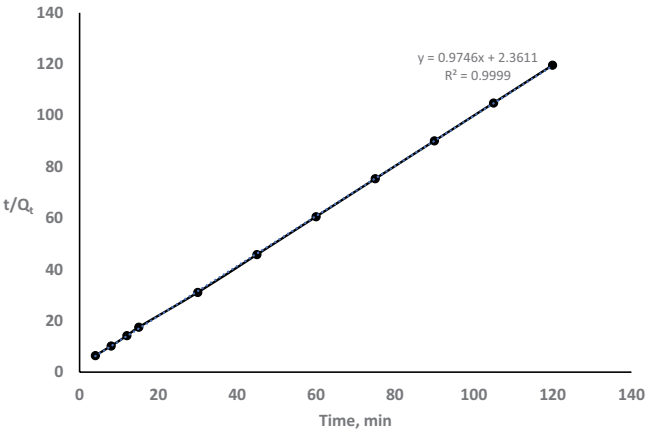

Fig. 12. Pseudo-second-order reaction kinetics: plot of t/Q_t vs. contact time.

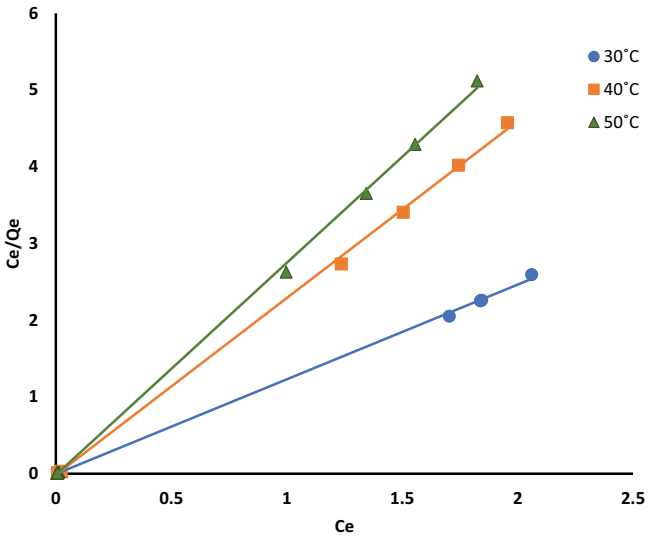

Fig. 13. Langmuir adsorption isotherm: plot of C_e/Q_e vs. C_e.

Table 1
Adsorption isotherm constants for the adsorption of Cs(I) using activated BCS

Adsorption isotherm	Constant	Temperature		
		30°C	40°C	50°C
Langmuir	K_L, L/mg	301	146.79	178
	Q_{max}, mg/g	0.8103	0.4339	0.3619
Freundlich	K_F, mg/g	1.784	2.156	2.633
	n, g/L	7.794	8.240	9.525
Dubinin–Radushkevich isotherm	K_{ad}, mol²/J²	5 × 10⁻⁹	4 × 10⁻⁹	3 × 10⁻⁹
	Q_{max}, mg/g	1.913	2.269	2.729
	E, kJ/mol	10.15	11.18	12.91

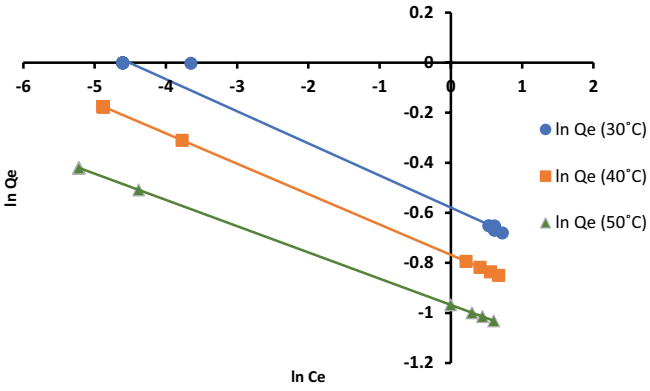

Fig. 14. Freundlich adsorption isotherm: plot of lnQ_e vs. lnC_e.

Freundlich adsorption isotherm. The values of n and K_F were evaluated from the slope and intercept of the plot. For the favourable adsorption isotherm, the n value should be in the range of 1–10. The calculated values of n are in the of 7–9 as shown in Table 1 and this indicates the favourable adsorption isotherm.

3.9.3. Dubinin–Radushkevich isotherm

The physical or chemical mechanism of the adsorption process could be identified with Dubinin–Radushkevich isotherm [51]. This isotherm is the superior model of the Langmuir adsorption isotherm and is also applied to study the porous structure of the adsorbent. The Dubinin–Radushkevich isotherm is given by Eq. (9) [52].

$$\ln Q_e = \ln Q_{max} - K_{ad}\varepsilon^2 \tag{9}$$

where Q_e is the adsorption capacity at equilibrium, Q_{max} is the maximum adsorption capacity, K_{ad} is the Dubinin–Radushkevich isotherm constant in mol²/J², and ε is the Polanyi potential.

The Polanyi potential, ε is given by Eq. (10):

$$\varepsilon = RT\ln\left(1+\frac{1}{C_e}\right) \tag{10}$$

where R is the gas law constant, T is the absolute temperature, and C_e is the equilibrium concentration of Cs(I). The

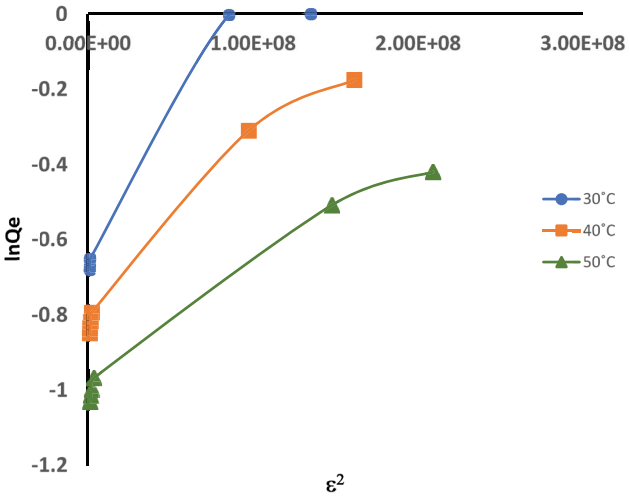

Fig. 15. Dubinin–Radushkevich isotherm: plot of lnQ_e vs. ε².

linear relation was observed between lnQ_e and ε² as shown in Fig. 15. The values of Q_{max} and K_{ad} were evaluated from the intercept and slope of the plot. The values are shown in Table 1. The mean free energy was evaluated from K_{ad} to find the adsorption mechanism. The mean free energy E is given by Eq. (11):

$$E = \frac{1}{\left(2K_{ad}\right)^2} \tag{11}$$

The value of mean free energy E in the range of 8–16 kJ/mol represents the adsorption involving chemical mechanism and the value less than 8 kJ/mol represents the adsorption process involving physical mechanism [52]. The values of E calculated from K_{ad} are shown in Table 1. It is observed from Table 1 that the free energy lies between 10 and 13 kJ/mol, which implies that the adsorption process involves a chemical mechanism.

4. Response surface methodology

Based on the batch experiments, the prime variables have been screened as contact time, initial pH, the dosage of activated BCS, and concentration of Cs(I). The higher and lower levels of the prime variables have been fixed based on the preliminary batch experiments. The following range of values was chosen for the process variables based on the design of experiments: contact time 1–100 min, initial pH of the solution 2–12, adsorbent dosage 0.05–5 g, and initial concentration of Cs(I) 1–20 mg/L. The set of experiments was performed as shown in Table 2 and evaluated the percentage removal of Cs(I) and adsorption capacity of activated BCS. The experimental data were analyzed and optimum parameters were obtained.

4.1. Interactive effect of contact time and initial solution pH

The 3D surface response plot is shown in Fig. 16. The percentage removal of cesium ion increases substantially

Table 2
Central composite design and the experimental response for the removal of Cs(I) using activated BCS

Run	Factor 1 *A*: Time (min)	Factor 2 *B*: Initial solution pH	Factor 3 *C*: Adsorbent dosage (g)	Factor 4 *D*: Initial concentration of Cs(I) (mg/L)	Percentage removal (%)	Adsorption capacity (mg/g)
1	100	12	2	1	86.66	0.01969
2	38	12	0.05	10	77.88	0.1772
3	50	7	2.5	20	87.54	0.3977
4	21	7	5	10	75.56	0.1786
5	1	2	0.05	20	23.64	0.1074
6	1	2	5	20	44.46	0.2020
7	95	7	4	11	85.56	0.2152
8	100	6.5	1	20	86.79	0.3945
9	1	9	0.05	1	36.45	0.008284
10	100	12	5	20	99.01	0.4500
11	50	7	2.5	20	87.35	0.3970
12	21	7	5	10.5	80.26	0.1897
13	1	7	1	12.5	85.83	0.2340
14	1	2	3	5	40.24	0.04389
15	1	2	3	5	40.24	0.04389
16	1	9	0.05	1	44.46	0.01010
17	100	2	5	1	50.15	0.01139
18	68	2	0.05	1	24.47	0.005561
19	1	12	5	1	68.85	0.01565
20	38	12	0.05	10	49.68	0.1102
21	1	12	3	20	99.10	0.4505
22	55	6	3	1	65.35	0.01485
23	100	6	0.05	10	45.05	0.09875
24	100	2	3	20	64.15	0.2915
25	100	12	0.05	20	60.11	0.2732

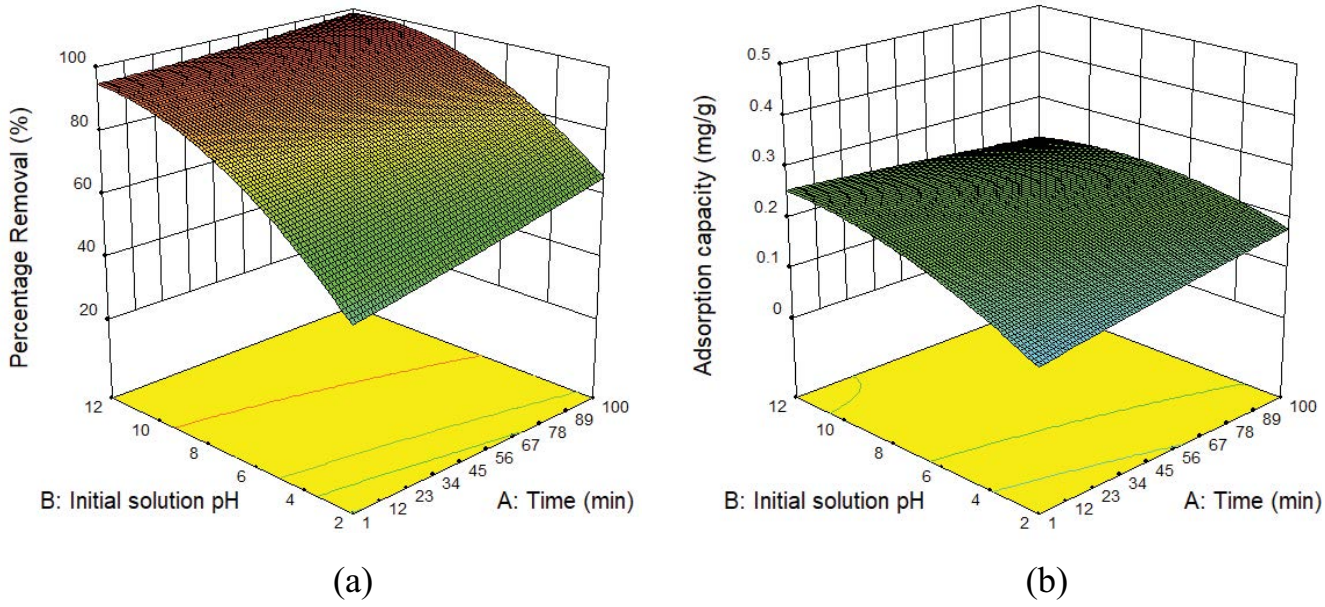

(a) (b)

Fig. 16. (a) Interactive effect of initial solution pH and contact time on the percentage removal of Cs(I) and (b) interactive effect of initial solution pH and contact time on the adsorption capacity of activated BCS.

with pH at a constant time and it reaches the maximum value of around 99% at pH 10–12 as illustrated in Fig. 16a. When we increase the solution pH, the active sites on the BCS acquire a negative charge and the electrostatic attraction between BCS and the cesium ions increases. Due to this, more removal has been pronounced at higher pH. It is also depicted from the figure that the effect of contact time at a constant initial pH does not have much influence on the percentage removal. The same effect is also observed for adsorption capacity. There is an observable influence of pH on adsorption capacity till the contact time of 12 min as shown in Fig. 16b. From the ANOVA table (Tables 3 and 4), it is observed that the *p*-value is less than 0.05, which indicates the interactive influence of solution pH and contact time on the adsorption capacity of activated BCS.

4.2. Interactive effect of contact time and adsorbent dosage

The influence of contact time and the dosage of activated BCS is shown in Fig. 17. The percentage removal of cesium ions increases with adsorbent dosage up to 3.5 g, at a constant time and beyond that, it drops down to 70% removal of Cs(I). As we increase the dosage of activated BCS, the availability of active pores increases, which is reflected by the increase in the percentage removal of Cs(I) with the adsorbent dosage up to 3.5 g. However, with a further increase in the dosage of activated BCS, the percentage removal of Cs(I) falls due to the insufficient availability of the cesium ions. The increase in the percentage removal of Cs(I) with the contact time at a constant dosage of activated BCS is not quite prominent as depicted in Fig. 17a. Since the adsorption capacity is interconnected with the percentage removal, the same tendency is noticed for the interactive influence of dosage of activated BCS and contact time on the adsorption capacity of BCS as exhibited in Fig. 17b. It is observed from the *p*-value shown in ANOVA table (Tables 3 and 4) that there is a remarkable influence of adsorbent dosage on the percentage removal as well as the adsorption capacity of activated BCS.

4.3. Interactive effect of initial concentration of cesium ion and contact time

The 3D surface plot representing the interactive influence of the concentration of Cs(I) and contact time is shown in Fig. 18. The percentage removal of Cs(I) rises gradually with the increase in the concentration of Cs(I), at a constant contact time. With the increase in the cesium concentration, due to the availability of adequate cesium ions, the percentage removal increases. It is also depicted in Fig. 18b that there is a steep rise in the adsorption capacity with the increase in the cesium concentration. Concerning the contact time, there is no noteworthy effect on percentage removal and adsorption capacity. This could also be confirmed by the *p*-value of the ANOVA table (Tables 3 and 4).

4.4. Interactive effect of adsorbent dosage and initial solution pH

The interactive impact of the dosage of activated BCS and solution pH on the removal of cesium is illustrated in Fig. 19. With the increase in pH at the constant dosage of activated BCS the percentage removal of Cs(I) and also

Table 3
ANOVA table for the percentage removal of Cs(I)

Source	Sum of squares	df	Mean square	*F*-value	*p*-value Prob. > *F*	
Model	11,766.27	14	840.45	8.48	0.0009	Significant
A-Time	390.64	1	390.64	3.94	0.0751	
B-Initial solution pH	4,856.51	1	4,856.51	49.03	<0.0001	
C-Adsorbent dosage	2,060.83	1	2,060.83	20.80	0.0010	
D-Initial concentration of cesium	1,122.17	1	1,122.17	11.33	0.0072	
AB	99.97	1	99.97	1.01	0.3388	
AC	43.70	1	43.70	0.44	0.5216	
AD	88.90	1	88.90	0.90	0.3658	
BC	45.55	1	45.55	0.46	0.5131	
BD	11.09	1	11.09	0.11	0.7448	
CD	3.58	1	3.58	0.04	0.8531	
A^2	1.17	1	1.17	0.01	0.9155	
B^2	434.54	1	434.54	4.39	0.0627	
C^2	1,563.10	1	1,563.10	15.78	0.0026	
D^2	148.30	1	148.30	1.50	0.2492	
Residual	990.61	10	99.06			

Table 4
ANOVA table for the adsorption capacity of activated BCS

Source	Sum of squares	df	Mean square	*F*-value	*p*-value Prob. > *F*	
Model	0.55	14	0.04	33.05	<0.0001	Significant
A-Time	1.123×10^{-3}	1	1.123×10^{-3}	0.94	0.3541	
B-Initial solution pH	0.03	1	0.03	23.48	0.0007	
C-Adsorbent dosage	0.01	1	0.01	9.47	0.0117	
D-Initial concentration of cesium	0.38	1	0.38	322.99	<0.0001	
AB	8.160×10^{-3}	1	8.160×10^{-3}	6.86	0.0257	
AC	3.114×10^{-4}	1	3.114×10^{-3}	0.26	0.6201	
AD	6.993×10^{-4}	1	6.993×10^{-3}	0.59	0.4610	
BC	1.038×10^{-3}	1	1.038×10^{-3}	0.87	0.3723	
BD	0.02	1	0.02	15.64	0.0027	
CD	6.502×10^{-3}	1	6.502×10^{-3}	5.46	0.0415	
A^2	1.708×10^{-5}	1	1.708×10^{-3}	0.01	0.9070	
B^2	4.324×10^{-3}	1	4.324×10^{-3}	3.63	0.0857	
C^2	0.02	1	0.02	12.82	0.0050	
D^2	2.339×10^{-5}	1	2.339×10^{-5}	0.02	0.8913	
Residual	0.01	10	1.190×10^{-3}			

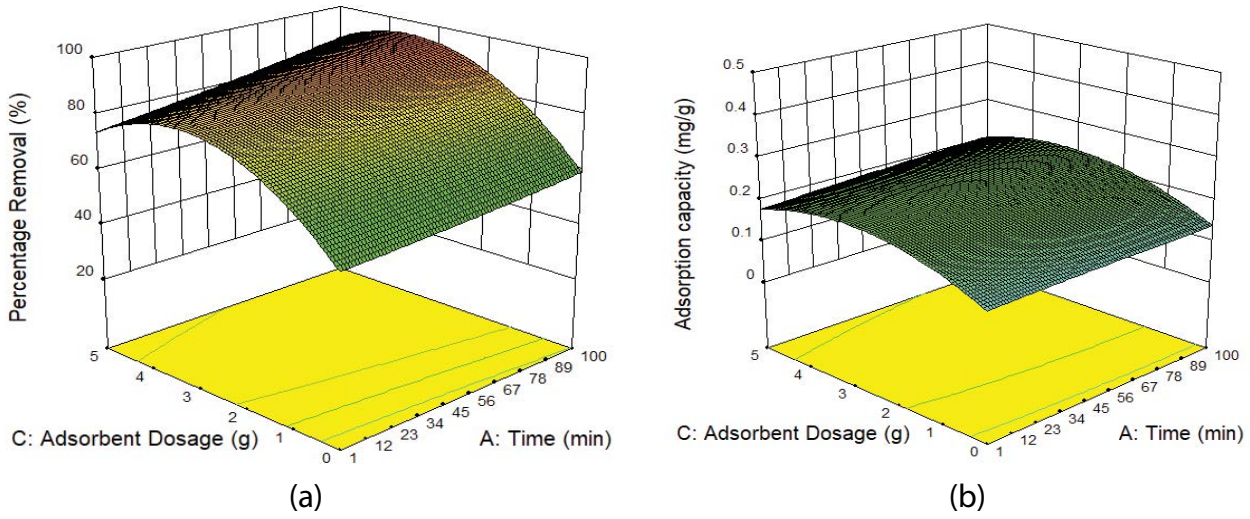

Fig. 17. (a) Interactive effect of adsorbent dosage and contact time on the percentage removal of Cs(I) and (b) interactive effect of adsorbent dosange and contact time on the adsorption capacity of activated BCS.

adsorption capacity of activated BCS increases. However, beyond pH 8, there is no change in the percentage removal of Cs(I) and adsorption capacity. Since, at higher solution pH, the active sites on the BCS acquire a negative charge leading to the electrostatic attraction between BCS and the cesium ions, the percentage removal of cesium ions and adsorption capacity increases. Similarly, with the increase in the dosage of activated BCS at a constant pH the percentage removal and adsorption capacity increase. This is observed up to the adsorbent dosage of 3 g and a further increase in the adsorbent dosage has no impact on the percentage removal of Cs(I) and adsorption capacity. Since there is no adequate availability of cesium ions to get adsorbed by BCS, beyond the adsorbent dosage of 3 g, it does not show any impact on the removal of cesium ions. The impact of pH and also the dosage of activated BCS on the percentage removal of Cs(I) and adsorption capacity of activated BCS could be confirmed from the *p*-value of the ANOVA table (Tables 3 and 4).

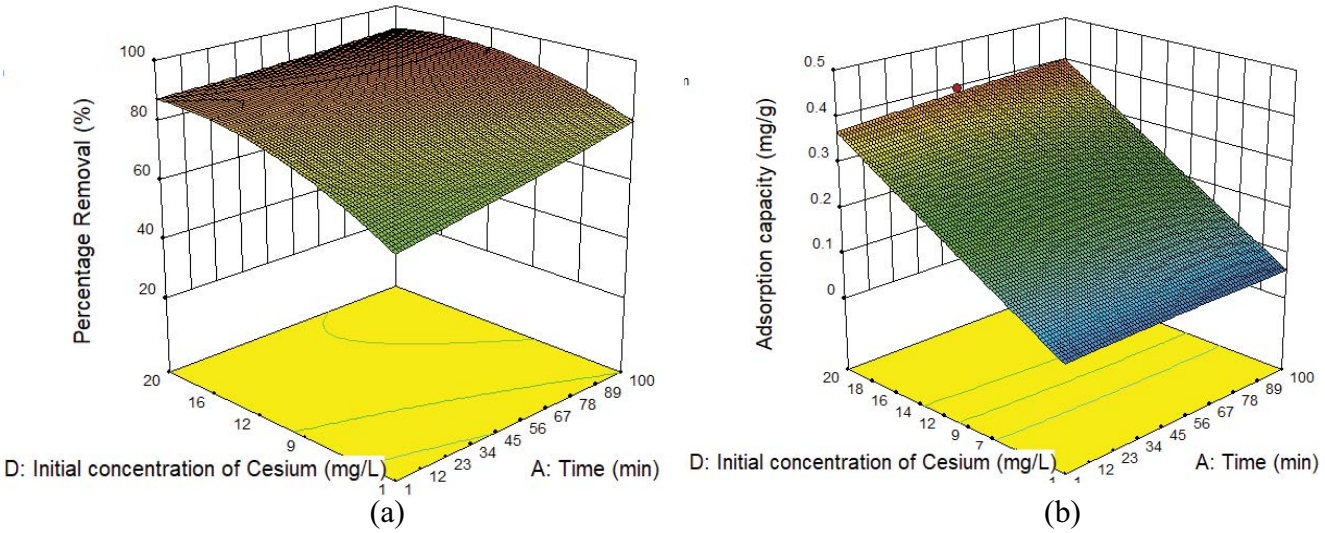

Fig. 18. (a) Interactive effect of initial concentration of Cs(I) and contact time on the percentage removal of Cs(I) and (b) interactive effect of initial concentration of Cs(I) and contact time on the adsorption capacity of activated BCS.

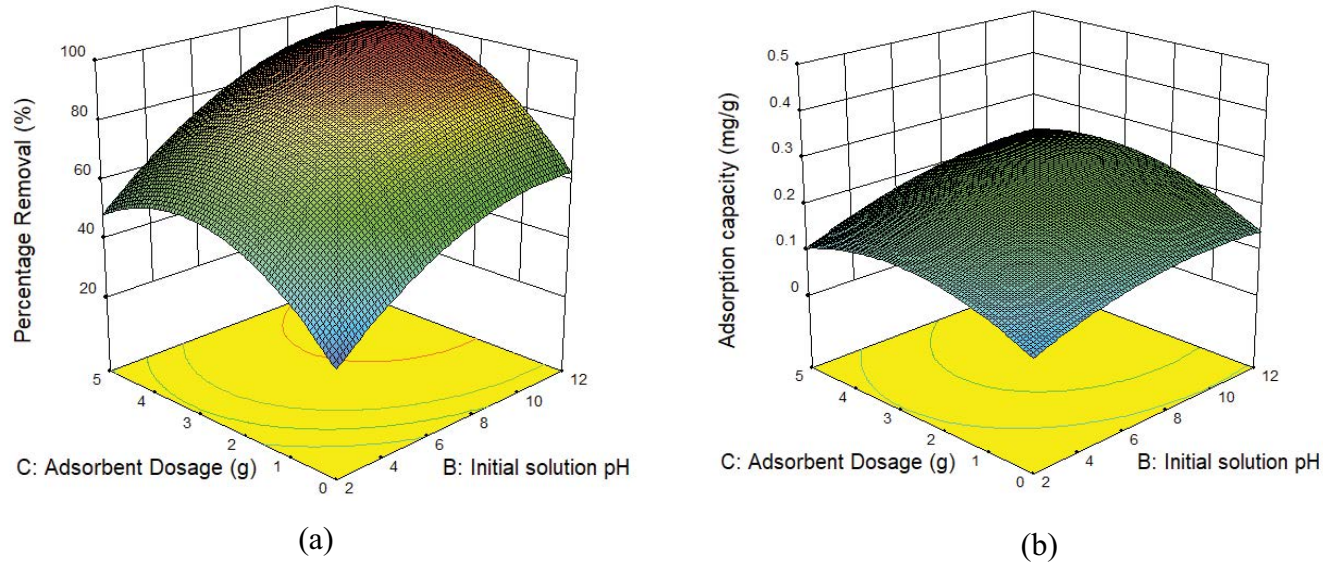

Fig. 19. (a) Interactive effect of adsorbent dosage and initial solution pH on the percentage removal of Cs(I) and (b) interactive effect of adsorbent dosage and initial solution pH on the adsorption capacity of activated BCS.

4.5. Interactive effect of initial concentration of cesium ion and initial solution pH

The 3D surface plot representing the interactive influence of the cesium concentration and pH on the percentage removal of cesium ion and adsorption capacity of activated BCS are shown in Fig. 20a and b. When we increase the concentration of Cs(I) at a constant pH, the percentage removal increases gradually up to 12 mg/L, and with a further increase, the percentage removal of Cs(I) remains constant. However, when we increase the concentration of Cs(I), due to adequate availability of cesium ions, a steep rise in the adsorption capacity of activated BCS is observed as shown in Fig. 20b.

4.6. Interactive effect of initial concentration of cesium ion and adsorbent dosage

The interactive effect of the concentration of Cs(I) and the dosage of activated BCS on the percentage removal of cesium ion and adsorption capacity of activated BCS are shown in Fig. 21a and b. The percentage removal of cesium ion and adsorption capacity of activated BCS are observed to increase up to the adsorbent dosage of 3 g and beyond that, there is a slight drop in the percentage removal and adsorption capacity. The percentage removal increases with the cesium concentration at a constant adsorbent dosage. This is observed till the concentration reaches 16 mg/L and with a further increase, there is no observable increase in the

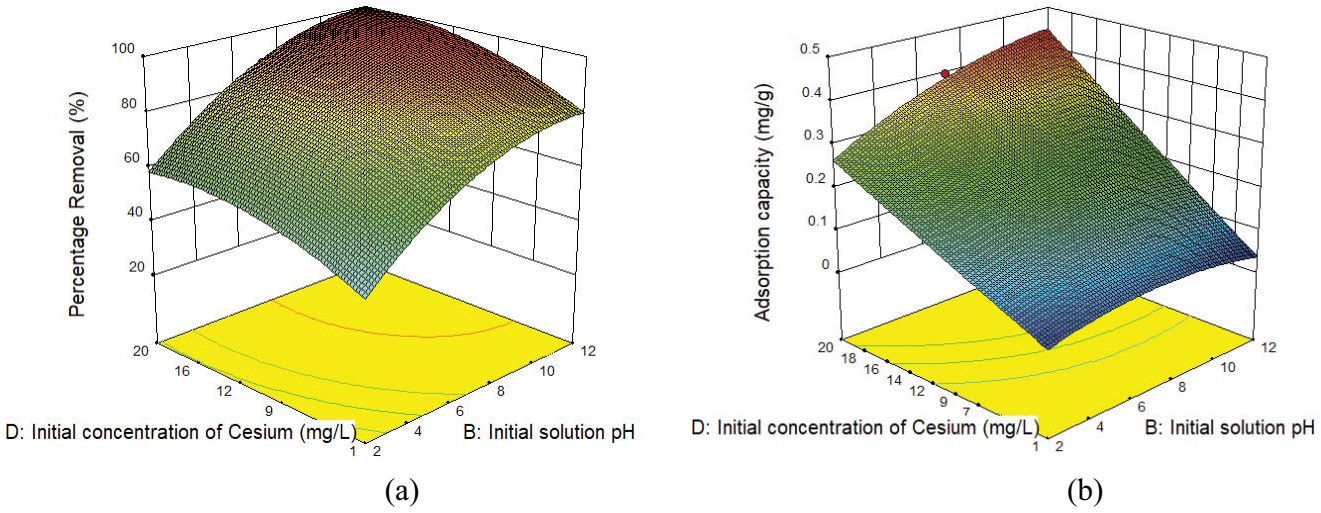

(a) (b)

Fig. 20. (a) Interactive effect of initial concentration of Cs(I) and initial solution pH on the percentage removal of Cs(I) and (b) interactive effect of initial concentration of Cs(I) and initial solution pH on the adsorption capacity of activated BCS.

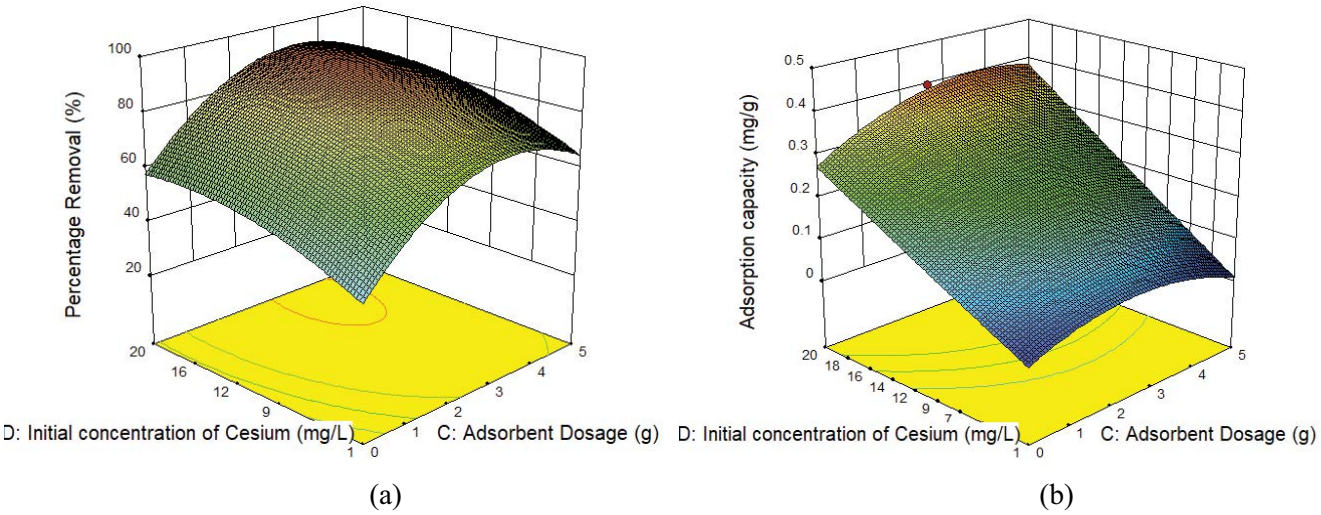

(a) (b)

Fig. 21. (a) Interactive effect of initial concentration of Cs(I) and adsorbent dosage on the percentage removal of Cs(I),and (b) interactive effect of initial concentration of Cs(I) and adsorbent dosage on the adsorption capacity of activated BCS.

Table 5
Optimized parameters for maximum percentage removal of Cs(I) and adsorption capacity of activated BCS

	Initial solution pH	Initial concentration of cesium ion (mg/L)	Contact time (min)	Adsorbent dosage (g)	Percentage removal of cesium ion (%)	Adsorption capacity of BCS (mg/g)
Cs(I)	10	17	15	3	100	0.415

percentage removal of cesium ion. Concerning the adsorption capacity of activated BCS, we could observe a sharp increase with the increase in the cesium concentration. The impact of adsorbent dosage on the percentage removal of cesium ion and adsorption capacity of activated BCS at a constant initial concentration of cesium ion is similar as depicted in Fig. 21b.

4.7. Optimization of process variables

The process variables initial solution pH, initial concentration of cesium ion, contact time, and adsorbent dosage were optimized and the values are given in Table 5. The maximum percentage removal of Cs(I) was obtained at the initial solution pH of 10, contact time of 15 min, initial concentration of 17 mg/L, and adsorbent dosage of 3 g.

5. Conclusions

The batch experiments were conducted for the separation of Cs(I) using activated BCS. The kinetic studies were performed and the experimental data were found to fit well with the pseudo-second-order kinetics. The adsorption isotherm studies were performed and the experimental data fit well with the Langmuir isotherm, Freundlich isotherm, and Dubinin–Radushkevich isotherm. The value of the Freundlich adsorption isotherm constant lies in the range of 7–9, which indicates the favourable adsorption isotherm. The adsorption mechanism was found to be chemical interaction through the Dubinin–Radushkevich isotherm model. The process modeling and optimization were performed using RSM and the following optimized process variables were obtained for nearly 100% removal of Cs(I) and 0.415 mg/g of adsorption capacity of activated BCS: initial solution pH–10, initial concentration of Cs(I) – 17 mg/L, contact time – 15 min, adsorbent dosage – 3 g. These values were validated through the experimental findings. The separation of Cs(I) by adsorption process using activated BCS as an adsorbent has been studied successfully, and with proper feasibility analysis, this technology could be implemented for large scale applications.

Acknowledgment

The authors would like to thank SRM Central Instrumentation Facility (SCIF), and Nanotechnology Research Centre (NRC), SRMIST, Kattankulathur, Tamil Nadu, India for the SEM, EDX, XRD and FTIR analysis.

References

[1] T. Subba Rao, S. Panigrahi, P. Velraj, Chapter 21 – Transport and Disposal of Radioactive Wastes in Nuclear Industry, S. Das, H.R. Dash, Eds., Microbial Biodegradation and Bioremediation: Techniques and Case Studies for Environmental Pollution, 2nd ed., Elsevier, Radarweg 29, P.O. Box: 211, 1000 AE Amsterdam, Netherlands, The Boulevard, Langford Lane, Kidlington, Oxford OX5 1GB, United Kingdom 50 Hampshire Street, 5th Floor, Cambridge, MA 02139, United States, 2022, pp. 419–440.

[2] F. Futagami, M. Soliman, K. Takamiya, S. Sekimoto, Y. Oki, T. Kubota, M. Konno, S. Mizuno, T. Ohtsuki, Isolation, characterization and source analysis of radiocaesium microparticles in soil sample collected from vicinity of Fukushima Dai-ichi nuclear power plant, J. Environ. Radioact., 223–224 (2020) 106388, doi: 10.1016/j.jenvrad.2020.106388.

[3] R. Jalali-Rad, H. Ghafourian, Y. Asef, S.T. Dalir, M.H. Sahafipour, B.M. Gharanjik, Biosorption of cesium by native and chemically modified biomass of marine algae: introduce the new biosorbents for biotechnology applications, J. Hazard. Mater., 116 (2004) 125–134.

[4] J.H. Song, T.J. Kim, J.-W. Yeon, Radioactivity data analysis of ^{137}Cs in marine sediments near severely damaged Chernobyl and Fukushima nuclear power plants, Nucl. Eng. Technol., 52 (2020) 366–372.

[5] G.E. Eperon, T. Leijtens, K.A. Bush, R. Prasanna, T. Green, J.T.-W. Wang, D.P. Mcmeekin, G. Volonakis, R.L. Milot, R. May, A. Palmstrom, D.J. Slotcavage, R.A. Belisle, J.B. Patel, E.S. Parrott, R.J. Sutton, W. Ma, F. Moghadam, B. Conings, A. Babayigit, H.-G. Boyen, S. Bent, F. Giustino, L.M. Herz, M.B. Johnston, M.D. Mcgehee , H.J. Snaith, Perovskite-perovskite tandem photovoltaics with optimized band gaps, Science, 354 (2016) 861–865.

[6] Y. Yu, X. Chen, Y. Jin, Z. Wu, Y. Yu, W. Lin, H. Yang, Electron-transporting layer doped with cesium azide for high-performance phosphorescent and tandem white organic light-emitting devices, J. Phys. D: Appl. Phys., 50 (2017) 275104, doi: 10.1088/1361-6463/aa72d2.

[7] J. Wang, S. Zhuang, Cesium separation from radioactive waste by extraction and adsorption based on crown ethers and calixarenes, Nucl. Eng. Technol., 52 (2020) 328–336.

[8] X. Liu, G.R. Chen, D.J. Lee, T. Kawamoto, H. Tanaka, M.L. Chen, Y.K. Luo, Adsorption removal of cesium from drinking waters: a mini review on use of biosorbents and other adsorbents, Bioresour. Technol., 160 (2014) 142–149.

[9] T. Yuan, Q. Chen, X. Shen, Adsorption of cesium using mesoporous silica gel evenly doped by Prussian blue nanoparticles, Chin. Chem. Lett., 31 (2020) 2835–2838.

[10] H. Kazemian, H. Zakeri, M.S. Rabbani, Cs and Sr removal from solution using potassium nickel hexacyanoferrate impregnated zeolites, J. Radioanal. Nucl. Chem., 268 (2006) 231–236.

[11] J. Zhang, L. Yang, T. Dong, F. Pan, H. Xing, H. Liu, Kinetics-controlled separation intensification for cesium and rubidium isolation from Salt Lake brine, Ind. Eng. Chem. Res., 57 (2018) 4399–4406.

[12] S. Liu, H. Liu, Y. Huang, W. Yang, Solvent extraction of rubidium and cesium from salt lake brine with t-BAMBP–kerosene solution, Trans. Nonferrous Met. Soc. China, 25 (2015) 329–334.

[13] G. Huang, P. Dou, Z. Zhang, J. Yan, Removal of cobalt from liquid radioactive waste by in situ electrochemical synthesis of ferrite, J. Radioanal. Nucl. Chem., 316 (2018) 61–70.

[14] E. Kavitha, M. Dalmia, A.M. Samuel, S. Prabhakar, M.P. Rajesh, Modeling and optimization of removal of strontium and cesium from aqueous streams by size enhanced ultrafiltration using chitosan derivative, Desal. Water Treat., 185 (2020) 262–276.

[15] S. Chen, J. Hu, S. Han, Y. Guo, N. Belzile, T. Deng, A review on emerging composite materials for cesium adsorption and environmental remediation on the latest decade, Sep. Purif. Technol., 251 (2020) 117340, doi: 10.1016/j.seppur.2020.117340.

[16] T.A. Saleh, G. Fadillah, E. Ciptawati, M. Khaled, Analytical methods for mercury speciation, detection, and measurement in water, oil, and gas, TrAC, Trends Anal. Chem., 132 (2020) 116016, doi: 10.1016/j.trac.2020.116016.

[17] T.A. Saleh, Nanomaterials: classification, properties, and environmental toxicities, Environ. Technol. Innovation, 20 (2020) 101067, doi: 10.1016/j.eti.2020.101067.

[18] T.A. Saleh, Protocols for synthesis of nanomaterials, polymers, and green materials as adsorbents for water treatment technologies, Environ. Technol. Innovation, 24 (2021) 101821, doi: 10.1016/j.eti.2021.101821.

[19] Y. Seo, Y. Hwang, Prussian blue immobilized on covalent organic polymer-grafted granular activated carbon for cesium adsorption from water, J. Environ. Chem. Eng., 9 (2021) 105950, doi: 10.1016/j.jece.2021.105950.

[20] D. Yang, H. Liu, Z. Zheng, S. Sarina, H. Zhu, Titanate-based adsorbents for radioactive ions entrapment from water, Nanoscale, 5 (2013) 2232–2242.

[21] J. Van R. Smit, Ammonium salts of the heteropolyacids as cation exchangers, Nature, 181 (1958) 1530–1531.

[22] H. Mimura, M. Saito, K. Akiba, Y. Onodera, Selective uptake of cesium by ammonium tungstophosphate (AWP) - calcium alginate composites, Solvent Extr. Ion Exch., 18 (2000) 1015–1027.

[23] A. Nilchi, H. Atashi, A.H. Javid, R. Saberi, Preparations of PAN-based adsorbers for separation of cesium and cobalt from radioactive wastes, Appl. Radiat. Isot., 65 (2007) 482–487.

[24] D. Song, S.-J. Park, H.W. Kang, S. Bin Park, J.-I. Han, Recovery of lithium(I), strontium(II), and lanthanum(III) using Ca–alginate beads, J. Chem. Eng. Data, 58 (2013) 2455–2464.

[25] Y. Kim, Y.K. Kim, J.H. Kim, M.-S. Yim, D. Harbottle, J.W. Lee, Synthesis of functionalized porous montmorillonite via solid-state NaOH treatment for efficient removal of cesium and strontium ions, Appl. Surf. Sci., 450 (2018) 404–412.

[26] B. Park, S.M. Ghoreishian, Y. Kim, B.J. Park, S.-M. Kang, Y.S. Huh, Dual-functional micro-adsorbents: application for simultaneous adsorption of cesium and strontium, Chemosphere, 263 (2021) 128266, doi: 10.1016/j.chemosphere.2020.128266.

[27] H.R. Yu, J.Q. Hu, Z. Liu, X.J. Ju, R. Xie, W. Wang, L.Y. Chu, Ion-recognizable hydrogels for efficient removal of cesium ions from aqueous environment, J. Hazard. Mater., 323 (2017) 632–640.
[28] N.D. Shooto, P.M. Thabede, E.B. Naidoo, Simultaneous adsorptive study of toxic metal ions in quaternary system from aqueous solution using low cost black cumin seeds (*Nigella sativa*) adsorbents, S. Afr. J. Chem. Eng., 30 (2019) 15–27.
[29] S. Sujatha, V. Govindan, R. Sivarethinamohan, Principal determinants of toxicity reduction by de-oiled soya using multivariate statistics: principal component analysis and multiple linear regression analysis, Appl. Ecol. Environ. Res., 15 (2017) 1717–1737.
[30] V. Gupta, P.I. Ali, Utilisation of bagasse fly ash (a sugar industry waste) for the removal of copper and zinc from wastewater, Sep. Purif. Technol., 18 (2000) 131–140.
[31] I.A. Kuti, B.A. Adabembe, M.O. Ogunwole, Production and characterization of bamboo activated carbon using different chemical impregnations for heavy metals removal in surface water, Niger. Res. J. Eng. Environ. Sci., 3 (2018) 177–182.
[32] I. Nhapi, N. Banadda, R. Murenzi, C.B. Sekomo, U.G. Wali, Removal of heavy metals from industrial wastewater using rice husks, Open Environ. Eng. J., 4 (2011) 170–180.
[33] K. Elgendy, S. Sobhy, M. Zaky, Removal of Some Heavy Metals From Sewage Water Using Natural and Modified Rice Straw, Conference: International Conference on Advances in Science (ICAS) 2017, 13–15 September, Istanbul, Turkey, 2017.
[34] E. Bernard, A. Jimoh, J.O. Odigure, Heavy metals removal from industrial wastewater by activated carbon prepared from coconut shell, Res. J. Chem. Sci., 3 (2013) 3–9.
[35] R. Baby, B. Saifullah, M.Z. Hussein, Palm kernel shell as an effective adsorbent for the treatment of heavy metal contaminated water, Sci. Rep., 9 (2019) 18955, doi: 10.1038/s41598-019-55099-6.
[36] U. Haripriyan, K.P. Gopinath, J. Arun, Chitosan based nano adsorbents and its types for heavy metal removal: a mini review, Mater. Lett., 312 (2022) 131670, doi: 10.1016/j.matlet.2022.131670.
[37] B. Kakavandi, A. Raofi, S.M. Peyghambarzadeh, B. Ramavandi, M.H. Niri, M. Ahmadi, Efficient adsorption of cobalt on chemical modified activated carbon: characterization, optimization and modeling studies, Desal. Water Treat., 111 (2018) 310–321.
[38] M. Ahmadi, H. Rahmani, B. Ramavandi, B. Kakavandi, Removal of nitrate from aqueous solution using activated carbon modified with Fenton reagents, Desal. Water Treat., 76 (2017) 265–275.
[39] N.D. Shooto, E.B. Naidoo, M. Maubane, Sorption studies of toxic cations on ginger root adsorbent, J. Ind. Eng. Chem., 76 (2019) 133–140.
[40] M. Ahmadi, B. Kakavandi, S. Jorfi, M. Azizi, Oxidative degradation of aniline and benzotriazole over PAC@$Fe^{II}Fe_2^{III}O_4$: a recyclable catalyst in a heterogeneous photo-Fenton-like system, J. Photochem. Photobiol., A, 336 (2017) 42–53.
[41] M. Kermani, J. Mehralipour, B. Kakavandi, Photo-assisted electroperoxone of 2,4-dichlorophenoxy acetic acid herbicide: kinetic, synergistic and optimization by response surface methodology, J. Water Process Eng., 32 (2019) 100971, doi: 10.1016/j.jwpe.2019.100971.
[42] H. Zeng, H. Hao, X. Wang, Z. Shao, Chitosan-based composite film adsorbents reinforced with nanocellulose for removal of Cu(II) ion from wastewater: preparation, characterization, and adsorption mechanism, Int. J. Biol. Macromol., 213 (2022) 369–380.
[43] J. Gao, L. Zhang, S. Liu, X. Liu, Enhanced adsorption of copper ions from aqueous solution by two-step DTPA-modified magnetic cellulose hydrogel beads, Int. J. Biol. Macromol., 211 (2022) 689–699.
[44] C. Cojocaru, G. Zakrzewska-Trznadel, Response surface modeling and optimization of copper removal from aqua solutions using polymer assisted ultrafiltration, J. Membr. Sci., 298 (2007) 56–70.
[45] E. Kavitha, A. Sowmya, S. Prabhakar, P. Jain, R. Surya, M.P. Rajesh, Removal and recovery of heavy metals through size enhanced ultrafiltration using chitosan derivatives and optimization with response surface modeling, Int. J. Biol. Macromol., 132 (2019) 278–288.
[46] S.S. Al-Shahrani, Treatment of wastewater contaminated with cobalt using Saudi activated bentonite, Alexandria Eng. J., 53 (2014) 205–211.
[47] T.A. Saleh, Isotherm, kinetic, and thermodynamic studies on Hg(II) adsorption from aqueous solution by silica- multiwall carbon nanotubes, Environ. Sci. Pollut. Res., 22 (2015) 16721–16731.
[48] T.A. Saleh, Simultaneous adsorptive desulfurization of diesel fuel over bimetallic nanoparticles loaded on activated carbon, J. Cleaner Prod., 172 (2018) 2123–2132.
[49] L. Liu, X.-B. Luo, L. Ding, S.-L. Luo, Chapter 4 – Application of Nanotechnology in the Removal of Heavy Metal From Water, X. Luo, F. Deng, Eds., Nanomaterials for the Removal of Pollutants and Resource Reutilization: Micro and Nano Technologies, Elsevier, Radarweg 29, P.O. Box: 211, 1000 AE Amsterdam, Netherlands, The Boulevard, Langford Lane, Kidlington, Oxford OX5 1GB, United Kingdom, 50 Hampshire Street, 5th Floor, Cambridge, MA 02139, United States, 2019, pp. 83–147.
[50] B. Zhang, B. Zhang, X. Liu, Chitosan coated – porous low expansion vermiculite for efficient removal of cesium from radioactive wastewater, Environ. Chem. Ecotoxicol., 3 (2021) 182–196.
[51] Y. Chen, Y. Zhu, Z. Wang, Y. Li, L. Wang, L. Ding, X. Gao, Y. Ma, Y. Guo, Application studies of activated carbon derived from rice husks produced by chemical-thermal process—a review, Adv. Colloid Interface Sci., 163 (2011) 39–52.
[52] H.H.A. Rahman, A.H.E. Moustafa, M.G. Kassem, Black cumin (*Nigella sativa*) as low cost biosorbent for the removal of toxic Cu(II) and Pb(II) from aqueous solutions, Int. J. Eng. Technol., 15 (2015) 46–66.